ACS OMEGA

http://pubs.acs.org/journal/acsodf

Article

Effect of Impurity Atoms on the Adsorption/Dissociation of Hydrogen Sulfide and Hydrogen Diffusion on the Fe(100) Surface

Jingxuan Liang, Xiangli Wen, Shikai Wei, and Shuqi Zheng*

Cite This: *ACS Omega* 2021, 6, 14701−14712

Read Online

ACCESS | Metrics & More | Article Recommendations | Supporting Information

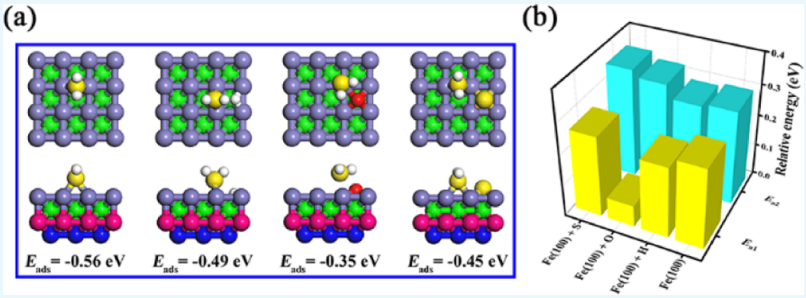

ABSTRACT: In the actual environment, impurity atoms significantly affect the adsorption/dissociation of gas molecules on the substrate surface and in turn promote or impede the formation of subsequent products. In this study, we investigate the effects of three kinds of impurity atoms (H, O, and S) on the adsorption/dissociation of hydrogen sulfide (H_2S) and hydrogen (H) diffusion processes by using the density functional theory method. We found that impurity atoms can change the charge density distribution of the surface and thus affect the adsorption/dissociation process of H_2S. The existence of a H atom reduces the dissociation barrier of H_2S. The adsorption site of H_2S near the O atom is transferred from the bridge site to the adjacent top site and the first-order dissociation barrier of H_2S is 0.07 eV, which is prominently lower than that of the pristine surface (0.28 eV). The presence of a S atom transfers the adsorption site of H_2S to a farther bridge site and effectively affects the dissociation process of H_2S. Both O and S atoms hinder the dissociation process of HS. Moreover, the diffusion process of H atoms to the subsurface can be slightly impeded by the O atom. Our work theoretically explains the influence mechanism of impurity atoms on the adsorption/dissociation of H_2S and H diffusion behavior on the Fe(100) surface.

1. INTRODUCTION

The interaction of H_2S with iron is significant in many different domains. For instance, in the universe, a large amount of H_2S reacts with iron to form iron sulfide in the solar nebula, dramatically affecting the properties of planets and other objects constituted later.[1] On the earth, sulfate-reducing bacteria degrade the sulfur in the deposited organic matter to produce H_2S,[2,3] which mainly exists in the sewage environment, oil and gas field environment, as well as deep-sea ecosystem.[4] H_2S is the primary source of sulfur in acid gas mixtures.[5] In acid gases containing H_2S, metallic materials are prone to pitting corrosion, local corrosion, uniform corrosion, linear corrosion, stress corrosion cracking, and hydrogen-induced cracking.[6] Since the dissociation of H_2S is very favorable in thermodynamics, the H−S bond is relatively weak.[7] Consequently, the dissociation energy barrier of H_2S on many metal surfaces is generally small, such as iron. It leads to the rapid deposition of sulfur on the metal surface and subsequently forms sulfide.[8,9] Besides, H_2S can also be used as a "poisoning agent" to impede the process of combining H atoms into H_2, thereby making the diffusion process of H atoms into the body structure more pronounced, especially in iron-based alloys.[10,11]

At present, the corrosion behavior of steel in a H_2S environment has been investigated extensively in the experiment. However, due to the complexity of the electronic structure, terminal atoms, and stability of the surface and interface, it is relatively difficult to determine the interaction between small molecules and low-dimensional surfaces from the microscopic perspective through existing experimental techniques. With the promotion of the application of first principles, using computers as an auxiliary tool provides us a new concept to work out related problems in materials science by constructing related models. This method can not only reduce costs but also replace some complicated and dangerous experiments, thereby solving some problems that cannot be

Received: April 12, 2021
Accepted: May 20, 2021
Published: May 28, 2021

ACS Publications

© 2021 The Authors. Published by American Chemical Society

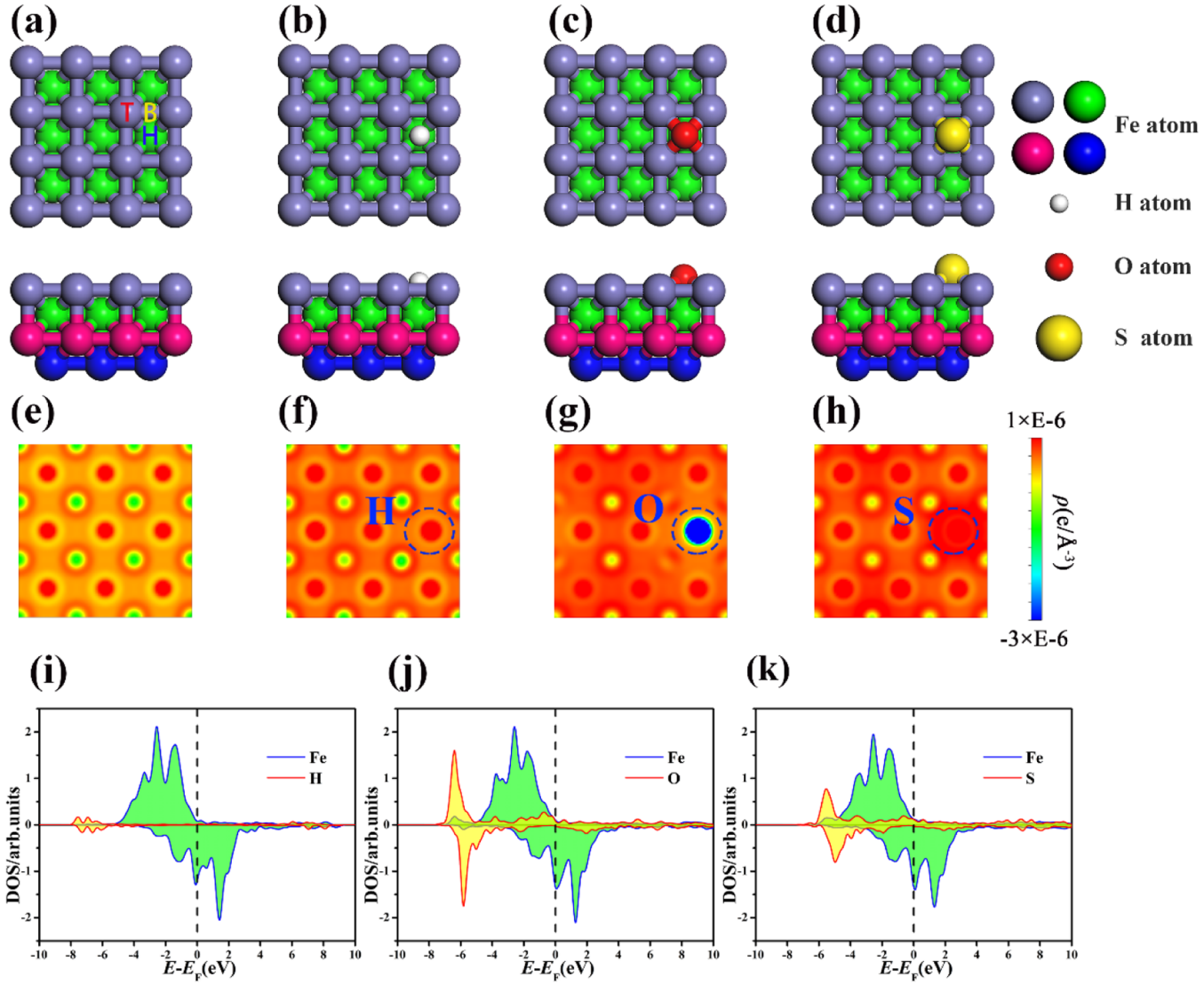

Figure 1. Top and front view of the different adsorption sites (a) and stable adsorption structure of H (b), O (c), and S (d) atoms on the surface; charge density distribution of the pristine (e) and those preadsorbed with H (f), O (g), and S (h) atom Fe(100) surfaces; PDOS of impurity atoms and Fe atoms: H and Fe (i), O and Fe (j), and S and Fe (k).

solved experimentally. Density functional theory (DFT) calculations can provide an understanding of the mutual effect between small inorganic/organic molecules and concrete surfaces at the molecular level. Over the past few years, DFT has been broadly applied to study the adsorption/dissociation process of molecules, electron structure, and charge transfer between molecules and the matrix.

In previous research, some academics examined the adsorption/dissociation process of H_2S on clean Fe(110) as well as Fe(100) surfaces and found that H_2S is more prone to dissociate on the Fe(110) surface.[12,13] Thereafter, the adsorption structure and electronic properties of H_2S on the Fe(100) surface were further reported.[14] Moreover, Feng-Chun et al. calculated the changes in the electronic properties of the matrix when different concentrations of H_2S interact with the Fe(111) surface and found that the interaction between the adsorbent and matrix gradually decreases with the increase of H_2S coverage.[15] Recently, Wen et al. investigated the impact of vacancy defects on the adsorption/dissociation of H_2S on the Fe(100) surface and drew the conclusion that vacancy defects had a significant contribution to promote the adsorption/dissociation of H_2S.[16]

Considering the concentration of gas, Jiao et al. studied the adsorption configuration of CO on the Fe(100) surface with high coverage rates and calculated the departure path.[17] Subsequently, Liu et al. suggested the adsorption and dissociation processes of H_2O with different coverage rates on Fe(110) and Fe(100) surfaces.[18,19] On the basis of these works, Liu et al. continued to study the competitive adsorption of CO and H_2O on different iron surfaces and proposed the reaction mechanism of water to gas.[20,21] These calculations all show that the adsorption and dissociation processes of gas molecules are significantly affected by the coverage rate.

Although predecessors have conducted detailed research studies on the interaction between small molecules and Fe, most of their studies focus on clean iron surfaces and have not considered the effects of other atoms existing in the actual environment. Generally speaking, there are many H and O atoms in the actual environment, while the ubiquitous H_2S, H_2O, H_2, and O_2 will also produce many H, O, and S atoms after they are adsorbed and dissociated on the surface of iron

https://doi.org/10.1021/acsomega.1c01946
ACS Omega 2021, 6, 14701−14712

or ferric sulfide. Then, these atoms may be adsorbed on the surface. As a matter of fact, impurity atoms will significantly affect the adsorption/dissociation of gas molecules on the surface. For example, the existence of an O atom will not only decrease the dehydrogenation barrier of CH_3OH, CH_3O, H_2COO, NH_3, and H_2O but also facilitate the dissociation of H_2 on the Cu(111) surface.[22,23] Abbasi et al. researched the adsorption/dissociation process of H_2S on TiO_2 anatase nanoparticles decorated by an N atom and found that the N atom would promote the adsorption of H_2S.[24] It can be seen that the impurity atoms on the matrix will affect the adsorption/dissociation of gas molecules. However, the adsorption/dissociation process of H_2S on an iron surface with impurity atoms has not been studied yet and the effect mechanism of the impurity atoms is still indistinct. Moreover, the corrosion behavior of iron with H_2S needs to be further supplemented theoretically.

In this work, using the DFT method, three kinds of impurity atoms are introduced in the adsorption/dissociation process of H_2S. We discussed the influence of H, O, and S atoms on the adsorption site, adsorption energy, dissociation path, and dissociation barrier of H_2S. Whereafter, the diffusion energy barrier of the H atom from the surface to the subsurface is calculated.

2. RESULTS AND DISCUSSION

2.1. Adsorption of Impurity Atoms on the Fe(100) Surface. The possible adsorption sites of the Fe(100) surface are illustrated in Figure 1a. In terms of the adsorption of molecules and atoms, there are three feasible sites: the bridge site (B), the top site (T), and the four-fold-hollow site (H). The adsorption energy and distance of H, O, and S atoms from the iron surface are listed in Table 1. By comparing the adsorption energy, it is found that the impurity H, O, and S atoms are all stably adsorbed at the hole sites around Fe atoms. The stable adsorption structure of H, O, and S atoms is visualized in Figure 1b–d.

Table 1. Adsorption Energy and Distance of H, O, and S Atoms from the Surface at Different Adsorption Sites, with d as the Shortest Distance between the Adsorbed Atoms and Fe Atoms

adsorbed atom	adsorbed site	d (Å)	E_{ads} (eV)
S	**H**	2.341	**−2.98**
	T	2.037	−1.28
	B	2.198	−1.89
O	**H**	2.048	**−3.39**
	T	1.637	−2.04
	B	1.811	−2.82
H	**H**	1.949	**−0.45**
	B	1.708	−0.40

The charge density distribution diagrams of pristine and preadsorbed Fe(100) surfaces are described in Figure 1e–h. The red and blue represent areas with higher and lower charge density, respectively. The charge density distribution of the Fe(100)−H surface is almost the same as that of the pristine surface. In contrast, the charge density distribution around the O atom is lower than that of the pristine surface, while the charge density distribution around the S atom is higher than that of the pristine surface. This is related to the electronegativity of the impurity atoms (H, O, and S) and the distance from the surface.

The partial density of states (PDOS) of impurity atoms and Fe atoms is described in Figure 1i–k. It can be seen that the 1s orbital of the H atom and the 3d orbital of the Fe atom hardly overlap, which indicates that the interaction between the H atom and Fe atom is very small. The 2p orbitals of both O and S atoms form overlapping peaks with the Fe atom at −4−−6 eV. Moreover, the energy levels of the orbitals of the O atom are lower than that of the S atom, while the overlap is more obvious. It indicates that the O atom is more firmly bound to the Fe(100) surface. The PDOS also explains why the adsorption energy of the O atom is greater than that of the S atom. The interaction between impurity atoms and the Fe(100) surface may lead to changes in the E_{ads} and E_a of H_2S.

2.2. Adsorption of H_2S. As mentioned above, there are three different adsorption sites and H_2S is competitively adsorbed among them. After H_2S is stably adsorbed on different surfaces, the adsorption energy is calculated. Table 2 lists the distance (d) between the Fe(100) surface and H_2S as well as the related geometric structure parameters.

Table 2. Structural Parameters and Adsorption Energy of H_2S at Different Adsorption Sites on the Pristine and Those Preadsorbed with H, O, and S Atom Fe(100) Surfaces

adsorption site and spatial orientation	d (Å)	d (H−S) (Å)	[a]HSH (°)	E_{ads} (eV)
pristine Fe(100)−H_2S				
B1[a]−V[b]	2.352	1.372; 1.373	92.084	**−0.56**
Fe(100)−H−H_2S				
T−V	2.401	1.358; 1.362	91.567	−0.39
T−P[c]	2.384	1.361; 1.361	91.500	−0.41
B_1−V	2.378	1.367; 1.375	92.088	**−0.49**
Fe(100)−O−H_2S				
B−P	3.950	1.350; 1.352	90.770	−0.06
T−P	2.463	1.357; 1.358	91.245	**−0.35**
Fe(100)−S−H_2S				
T−P	2.447	1.361; 1.362	90.791	−0.24
B_2[d]−V	2.332	1.367; 1.374	92.761	**−0.45**

[a]B_1: Represents the bridge site closest to the impurity atoms. [b]V: Represents the molecule vertical to the surface. [c]P: Represents the molecule parallel to the surface. [d]B_2: Represents the bridge site next to the impurity atoms.

On the Fe(100) surface, impurity atoms will affect the stable adsorption site and configuration of H_2S. Top and side views of H_2S stably adsorbed on the pristine and preadsorbed surfaces are described in Figure 2a–d. The adsorption site and configuration of H_2S on the Fe(100)−H surface are the same as that of the pristine surface. The H atom does not change the adsorption site of H_2S, which can still be stably adsorbed at the bridge site closest to the impurity H atom. Although the E_{ads} is lower than of the pristine surface, the difference is not massive. It manifests that the presence of an H atom can slightly decrease the adsorption capacity of H_2S.

https://doi.org/10.1021/acsomega.1c01946
ACS Omega 2021, 6, 14701−14712

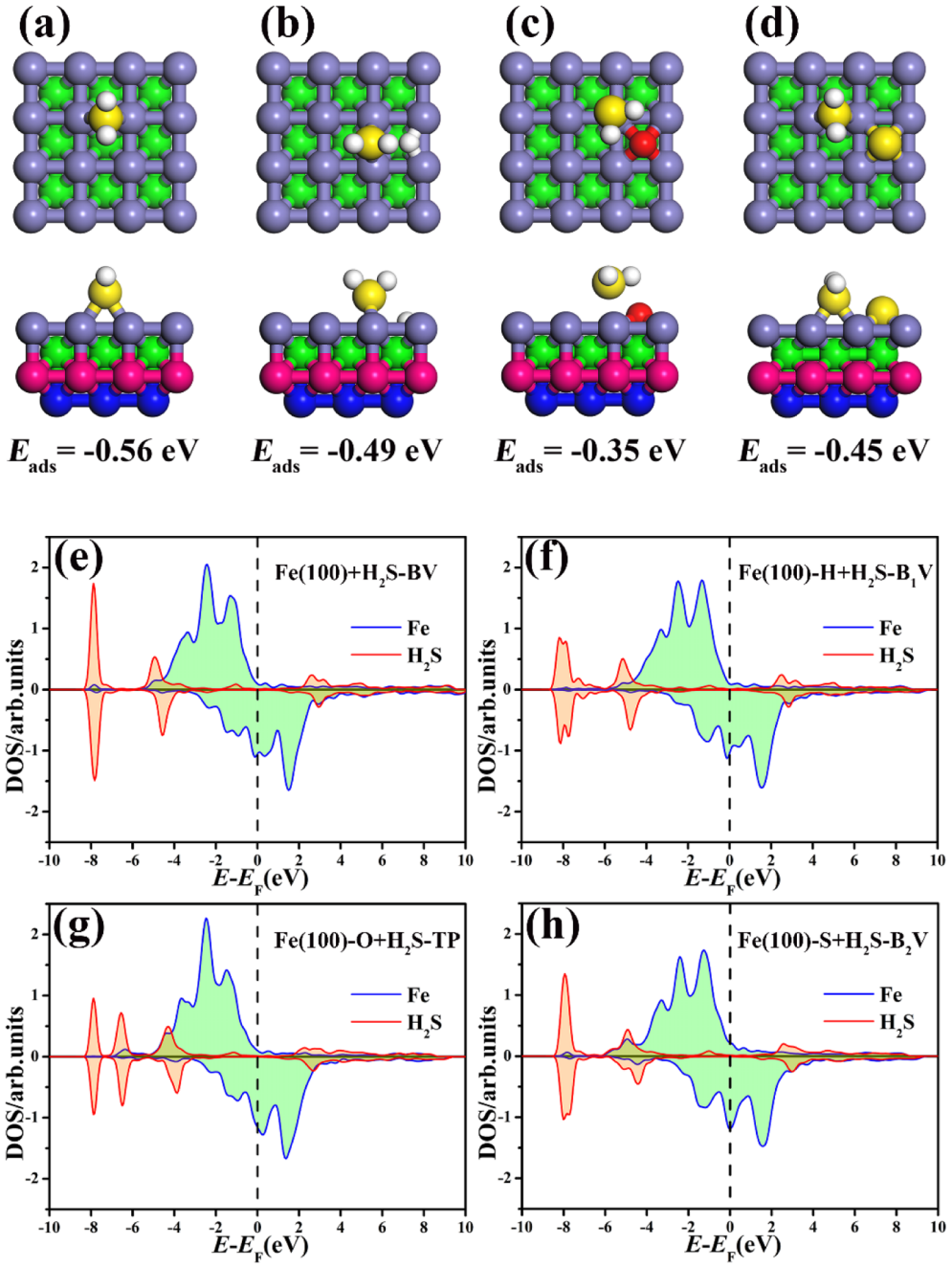

Figure 2. Top and front view of the stable adsorption configuration of H_2S on the pristine (a) and those preadsorbed with H (b), O (c), and S (d) atom Fe(100) surfaces; PDOS of H_2S and uppermost Fe atoms on different surfaces: H_2S is adsorbed on the pristine (e), H-atom-adsorbed (f), O-atom-adsorbed (g), and S-atom-adsorbed (h) Fe(100) surfaces.

However, the stable adsorption configuration of H_2S on Fe(100)−O and Fe(100)−S surfaces has changed compared to that of the pristine surface. The adsorption site of H_2S on the Fe(100)−O surface shifted from the bridge site closest to the O atom to the top site hithermost to the O atom. After that, the stable adsorption configuration changed from perpendicular to parallel to the surface, and besides, the distance from the surface increases slightly, which in turn leads to a decrease in the adsorption energy. This may be as a result of an absolute repulsive force between H_2S and the O atom. The stable adsorption conformation of H_2S on the Fe(100)−S surface changes significantly, which is transferred from the bridge site closest to the impurity S atom to the farther bridge site next to the impurity S atom. This is due to the fact that the S atom is far from the iron surface and there is a greater repulsion between H_2S and the S atom. Therefore, H_2S cannot be stably adsorbed at the bridge site or top site closest to the S atom and can only be transferred to the iron bridge site far away from the S atom.

By calculating the PDOS of the stable adsorption system and analyzing the electronic structure and bonding characteristics, the interaction between H_2S and the Fe(100) surface can be explained. The PDOS of the isolated H_2S and free surface slab model is visualized in Figure S1. The PDOS of the system after H_2S is stably adsorbed on different surfaces is exhibited in Figure 2e−h. According to Figure S1, one can find that H_2S

https://doi.org/10.1021/acsomega.1c01946
ACS Omega 2021, 6, 14701−14712

molecular orbitals can be refined into $1b_1$, $3a_1$, and $1b_2$ orbitals. They represent the characteristic orbitals of the lone pair of S vertical to the molecular plane, lone pair of electrons parallel to the molecular plane, and part of the H−S bond, respectively, which is similar to the H_2O molecular orbital.[25] Focusing on the PDOS distribution in Figure S1, it can be seen that the Fe(100) surface slab model has a partial contribution at −5−4 eV; additionally, the PDOS values of the separated H_2S are at −7 eV ($1b_2$), −5 eV ($3a_1$), and −2.5 eV ($1b_1$). The three peaks can be considered as energy levels isolated from each other. In addition, a smaller peak near 3 eV is included.

When H_2S is stably adsorbed on the pristine surface, the Fe orbitals in PDOS contribute around −5.5−5 eV, which is slightly lower than the energy level of the free surface. At the same time, H_2S contributes to the PDOS at −8, −6−−4, and 2−5 eV. Similarly, as portrayed in Figure 2f,h, after H_2S is stably adsorbed on Fe(100)−H and Fe(100)−S surfaces, the orbitals of H_2S are at −8, −6−−3, and 2−6 eV and Fe atoms contribute to the energy level of −6−6 eV. Beyond that, when H_2S is stably adsorbed on the Fe(100)−O surface, Fe atoms contribute around the −7−4 eV energy level, while H_2S has contribution values at −8, −6.5, −5−−3, and 2−6 eV.

By comparing the PDOS, it can be clearly observed that the molecular orbital position of H_2S transformed toward a lower region in all systems. This shows that H_2S has a certain degree of adsorption on the pristine and preadsorbed Fe(100) surfaces, while the adsorption will affect the electronic performance of the system. It can be seen from Figure 2e that the 3d orbital of the Fe atom and the $1b_1$ orbital of H_2S slightly overlap at −5.5−−3.5 eV, which indicates that there are electronic interactions in the system after the stable adsorption of H_2S, but the interaction force is small. Simultaneously, on the pristine and those pre-adsorbed with H or S atom Fe(100) surfaces, the $3a_1$ and $1b_1$ orbitals of H_2S overlap around −8.0 eV, forming the overlapping peaks. Nevertheless, $3a_1$ and $1b_1$ orbitals of H_2S did not form overlapping peaks on the Fe(100)−O surface and keep the PDOS shape similar to that in isolation, which shows that the reciprocity between S atoms in H_2S and Fe atoms is strong on the pristine and those preadsorbed with H and S atom Fe(100) surfaces. However, on the Fe(100)−O surface, the interaction between S atoms and Fe atoms is weak. The PDOS also explains the reason why the adsorption energy of H_2S is relatively small on the Fe(100)−O surface.

The calculation of the electronic structure argues that there is an inevitable electronic interaction between the Fe(100) surface and H_2S. The presence of H, O, and S atoms will have a certain impact on the interaction between H_2S and Fe, while the adsorption energy of H_2S on Fe(100)−H, Fe(100)−O, and Fe(100)−S surface is reduced to varying degrees compared to the pristine Fe(100) surface. The shift of the H_2S energy level in PDOS also shows that the presence of impurity atoms will make the adsorption configuration of H_2S more unstable compared with that of the pristine surface. It can be concluded that H, O, and S atoms will all hinder the adsorption of H_2S.

2.3. Dissociation of H_2S. To explore the influence of impurity atoms on the dissociation process of H_2S, climbing image nudged elastic band (CI-NEB) is applied to calculate the minimum energy paths (MEPs) and maximum dissociation E_a. The dissociation process of H_2S includes

$$(I)H_2S_{ads} \rightarrow H_{ads} + HS_{ads};\ (II)HS_{ads} \rightarrow H_{ads} + S_{ads}$$

For the purpose of obtaining MEPs, it is also necessary to understand the stable combination configuration of H + HS and H + S. Table 3 lists the related geometric parameters and

Table 3. Adsorption Energy, Adsorption Sites, and Structural Parameters of HS, H + HS, and H + S Stably Adsorbed on Different Fe(100) Surfaces

adsorption atom	adsorption site	d (Å)	d (H−S) (Å)	E_{ads}(eV)
		pristine Fe(100)		
HS	H	2.343	1.385	−3.86
H + HS	H + H	1.878; 2.339	1.378	−2.18
H + S	H + H	1.830; 2.342		−5.17
		Fe(100)−H		
HS	H	2.345	1.387	−3.86
H + HS	H + H	1.909; 2.344	1.388	−2.25
H + S	H + H	1.889; 2.319		−5.18
		Fe(100)−O		
HS	H	2.345	1.386	−3.82
H + HS	H + H	1.847; 2.344	1.388	−2.15
H + S	H + H	1.810; 2.319		−5.10
		Fe(100)−S		
HS	H	2.332	1.383	−3.86
H + HS	H + H	1.819; 2.329	1.383	−2.16
H + S	H + H	1.799; 2.309		−5.05

stable adsorption E_{ads} of the most stable adsorption structure, while other possible adsorption structures are listed in Table S1. Besides, the stable combination configuration of H + HS and H + S on different surfaces is presented in Figure 3. HS, S,

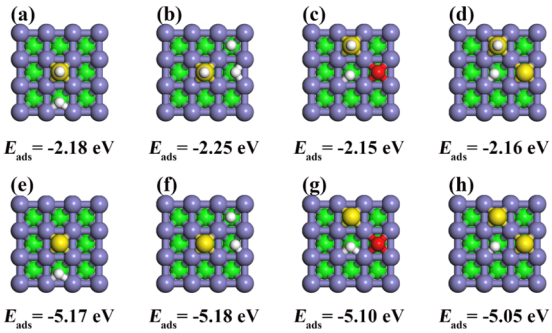

Figure 3. Top view of the stable combination configuration of H + HS and H + S on different surfaces.

and H are all stably adsorbed on the iron cavities on different surfaces. Impurity atoms will not change the stable adsorption site and adsorption conformation of HS, S, and H. The change of adsorption energy also shows that the H, O, and S atoms have little influence on the adsorption of HS, S, and H on the surface. Meanwhile, Table 4 lists the MEPs of the H_2S dissociation reaction and E_a and ΔE with and without the zero-point energy (ZPE) correction. The specific adsorption/dissociation process and the corresponding structures of IS_i, TS_i, and FS_i are exhibited in Figures S2 and 4−6.

The complete dissociation process of H_2S on the pristine Fe(100) surface is plotted in Figure S2. The energy barrier E_{a1} and E_{a2} calculated by us is very close to that calculated by Jiang et al.,[12] while the MEPs are consistent with the calculation result of Wen et al.,[16] thus proving the correctness of our work.

Subsequently, we investigated the effect of H, O, and S atoms on the dissociation of H_2S. First, on the Fe(100)−H

https://doi.org/10.1021/acsomega.1c01946
ACS Omega 2021, 6, 14701−14712

Table 4. Dissociation Energy (E_a) and Reaction Heat (ΔE) of the Fundamental Steps of H_2S Dissociation on the Pristine and Those Preadsorbed with Impurity Atom Fe(100) Surfaces

reaction coordinate	exclude ZPE correction		Include ZPE Correction	
	E_a (eV)	ΔE (eV)	E_{a-ZPE} (eV)	ΔE_{-ZPE} (eV)
pristine Fe(100) surface				
$Path_1$: $IS_1 \rightarrow TS_1 \rightarrow FS_1$	0.29	−1.30	**0.26**	−1.38
$Path_2$: $IS_2 \rightarrow FS_2$	N/A	−0.32	N/A	−0.33
$Path_3$: $IS_3 \rightarrow TS_3 \rightarrow FS_3$	0.33	−1.21	**0.30**	−1.24
$Path_4$: $IS_4 \rightarrow TS_4 \rightarrow FS_4$	0.09	−0.09	0.06	−0.10
Fe(100)−H surface				
$Path_1$: $IS_1 \rightarrow TS_1 \rightarrow FS_1$	0.22	−1.76	**0.23**	−1.85
$Path_2$: $IS_2 \rightarrow TS_2 \rightarrow FS_2$	0.34	−1.22	**0.29**	−1.25
$Path_3$: $IS_3 \rightarrow FS_3$	N/A	−0.10	N/A	−0.12
Fe(100)−O surface				
$Path_1$: $IS_1 \rightarrow TS_1 \rightarrow FS_1$	0.13	−1.81	**0.07**	−1.88
$Path_2$: $IS_2 \rightarrow TS_2 \rightarrow FS_2$	0.36	−1.23	**0.33**	−1.27
$Path_3$: $IS_3 \rightarrow TS_3 \rightarrow FS_3$	0.07	−0.04	0.05	−0.06
Fe(100)−S surface				
$Path_1$: $IS_1 \rightarrow TS_1 \rightarrow FS_1$	0.28	−1.71	**0.26**	−1.78
$Path_2$: $IS_2 \rightarrow TS_2 \rightarrow FS_2$	0.38	−1.16	**0.35**	−1.20
$Path_3$: $IS_3 \rightarrow TS_3 \rightarrow FS_3$	0.05	−0.03	0.03	−0.05

surface, the dissociation process of H_2S is divided into four steps (Figure 4): (1) H_2S (g) is adsorbed at the B-V position closest to the H atom. In comparison, the energy of the system is reduced by 0.49 eV after adsorption compared to the independent slab model; (2) by overcoming 0.23 eV of E_{a1}, the stably adsorbed H_2S dissociates into H + HS. H_2S breaks an HS bond at the pristine adsorption site by rotating the H atom closest to the impurity H atom directly into the iron surface (TS_1). Then, a H atom disengages and diffuses to the nearest hole site above the impurity H atom to form a bond, while HS directly diffuses to the nearest hole site to the left side of the adsorbed atom and forms a bond; (3) HS further overcomes E_{a2} (0.29 eV) and dissociates into H + S. After TS_2, the H atom diffuses to the bridge site and the S atom is still adsorbed at the pristine hole site; (4) the H atom moves to the hole site and this process does not need to overcome an energy barrier. It is found from Table 4 that on the Fe(100)−H surface, the dissociation E_{a1} (0.23 eV) and E_{a2} (0.29 eV) of H_2S are lower than those of the pristine surface, but the change is small. This indicates that the H atom will slightly promote the dissociation reaction of H_2S.

There are four steps used to describe the dissociation process of H_2S on the Fe(100)−O surface (Figure 5): (1) H_2S (g) is stably adsorbed at the T-P position closest to the O atom and the energy of the system after adsorption is reduced by 0.35 eV compared to that of the independent slab model; (2) by overcoming the E_{a1} of 0.07 eV, the stably adsorbed H_2S is decomposed into H + HS. H_2S breaks an HS bond by rotating to the lower left of the adsorption site. Then, a H atom separated from H_2S diffuses to the hole site closest to the left side of the impurity O atom to form a bond, while HS directly diffuses to the hole site closest to the adsorption site and forms a bond with the Fe atoms. (3) HS further overcomes E_{a2} (0.33 eV) and dissociates into H + S. After TS_2, the H atom diffuses to the bridge site and the S atom is still adsorbed at the primitive hole site; (4) finally, the H atom dissociated from HS diffuses to the more stable hole site through a smaller E_{a3} (0.05 eV).

The first-order dissociation barrier of H_2S on the Fe(100)−O surface is only 0.07 eV, which is significantly reduced compared to that on the pristine surface. This may be due to the different stable adsorption configurations, which also indicates that the existence of an O atom will facilitate the adsorption/dissociation process of H_2S. However, the dissociation process of HS is not very different from that of the pristine surface and the dissociation energy barrier increases slightly. Moreover, the energy barrier E_{a3} for the H atom to diffuse from the bridge site to the hole site is slightly reduced, indicating that the O atom has a specific hindering effect on the dissociation of HS. Nevertheless, the O atom still promotes the diffusion process of the H atom to the hole site.

Since there is a sizeable repulsive force between the S atom and H_2S molecule, H_2S cannot be adsorbed stably at the bridge or top site closest to the S atom. The stable adsorption configuration of H_2S has shifted to the B-V position next to the S atom. After the stable adsorption, by overcoming a 0.26 eV energy barrier, H_2S rotates vertically toward Fe atoms and dissociates into H + HS. Then, HS and H adsorb stably at the adjacent hole site, which is the same as the pristine surface. The dissociation process of HS is suppressed, but the diffusion process of the H atom is facilitated. It is indicated that both O and S atoms will hinder the dissociation of HS. Nevertheless, there is a promotion effect on the diffusion process of the H atom.

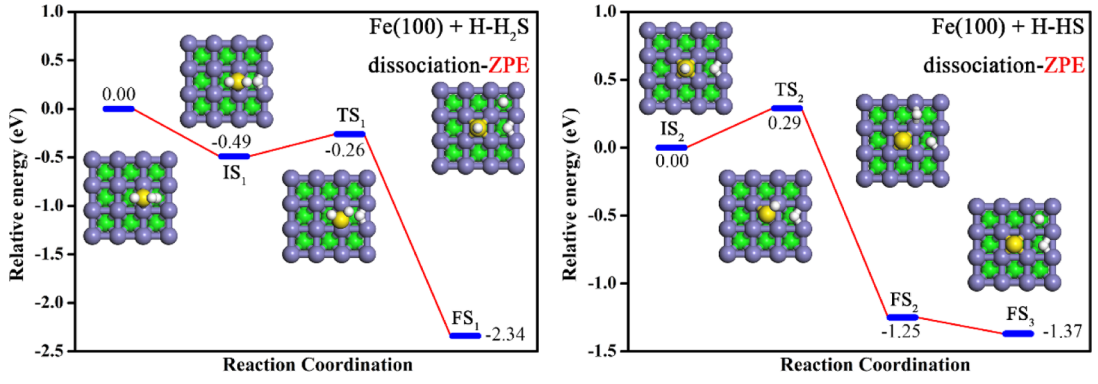

Figure 4. Top view of the intermediate state and the transition state (TS) of the most favorable path for the dissociation of H_2S on the Fe(100)−H surface, including ZPE correction.

https://doi.org/10.1021/acsomega.1c01946
ACS Omega 2021, 6, 14701−14712

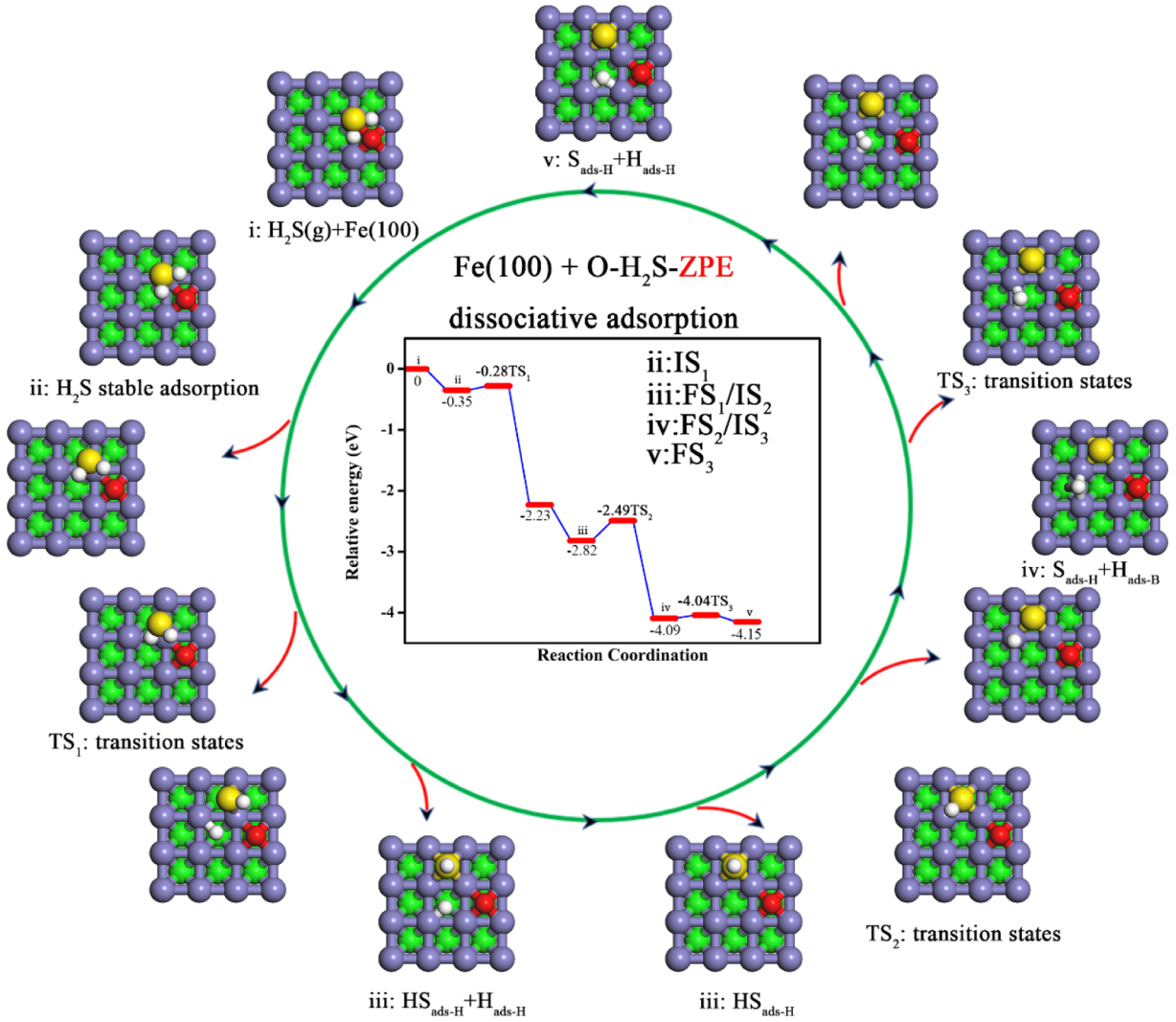

Figure 5. Top view of the intermediate state and the TS of the most favorable path for the dissociation of H_2S on the Fe(100)−O surface, including ZPE correction.

2.4. Effect of Impurity Atoms on H Diffusion. In recent years, DFT calculation has been widely used in the study of hydrogen storage and diffusion behavior.[26,27] The H atoms generated by H_2S dissociation can be steadily adsorbed at the hole site of the surface. By studying the diffusion process of the H atom, the understanding of hydrogen embrittlement can be further deepened. The adsorption/dissolution sites of the H atom are shown in Figure 7. H represents the hole site of the Fe(100) surface and G_1 and G_2 represent the tetrahedral gap dissolution sites of the first and second layer of Fe atoms, respectively. The diffusion process of the H atom from H to G_1, H to G_2, and G_1 to G_2 was studied by using the CI-NEB method. The dissolution energy barrier (E_{dif}) and reaction heat (ΔE) are listed in Table 5.

In all calculation results, it can be found that the diffusion barrier and reaction heat of the H atom from H to G_2 are relatively large, which indicates that this step is thermodynamically unfavorable, so it is difficult for the H atom to diffuse directly from H to G_2. On the pristine Fe(100) surface, by overcoming 0.38 eV of E_{dif-1}, the H atom diffuses from H to G_1. Subsequently, the H atom diffused from the tetrahedral gap of the first Fe atom to the tetrahedral gap of the second Fe atom by overcoming a greater energy barrier E_{dif-2} (0.56 eV). This process is identified as the rate-limiting step. The impurity H atom has a slight promotion effect on the H diffusion from H to G_1, but the energy barrier of the rate-limiting step is the same as the pristine surface. The impurity O atom will hinder the diffusion of the H atom from G_1 to G_2, and besides, the diffusion energy barrier E_{dif-2} increases to 0.62 eV. However, the energy barrier is not much different from the pristine surface (0.56 eV) and the impurity S atom also has little effect on the diffusion process.

Although impurity atoms will significantly affect the charge density of the surface and the adsorption/dissociation process of H_2S, it has little effect on the diffusion process of the H atom from the surface to the subsurface. It also depends on the distance between the H atom and the impurity atom and the influence range of the impurity atom.

2.5. Energy Barrier Split. The influence of impurity atoms on the dissociation of H_2S and the diffusion of the H atom are visualized in Figure 8. One can see that the impurity O atom dramatically facilitates the dissociation of H_2S; both the O atom and S atom will hinder the dissociation of HS. Furthermore, the diffusion process of the H atom is inhibited by O and S atoms, while the O atom has the most obvious inhibitory effect on this process.

https://doi.org/10.1021/acsomega.1c01946
ACS Omega 2021, 6, 14701−14712

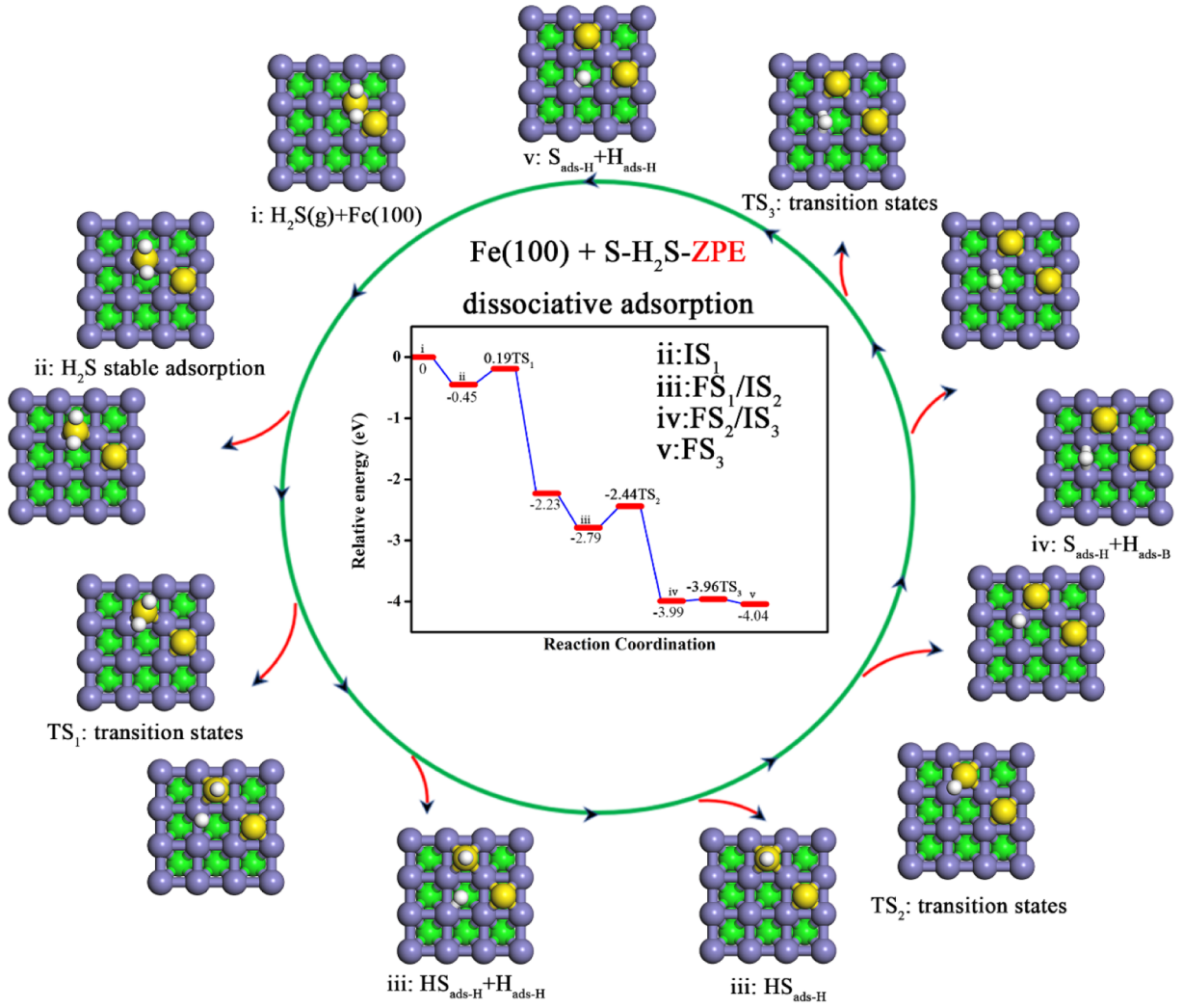

Figure 6. Top view of the intermediate state and the TS of the most favorable path for the dissociation of H_2S on the Fe(100)−S surface, including ZPE correction.

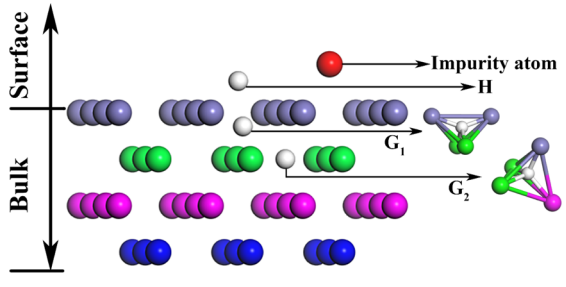

Figure 7. Diagram of adsorption/dissolution sites of H atoms on the surface and subsurface of Fe(100).

To further explore the impact of the impurity atoms, the contribution of each part to the dissociation E_a is calculated during the dissociation process, which is listed in Tables 6 and 7. According to the analysis of the results in the table, it is found that for the first-order dissociation of H_2S, the changes of each part contribute to the dissociation energy barrier, but the change of ΔE_{slab} has a negligible influence on the dissociation energy barrier. Similarly, the change in the distortion energy of H_2S is not apparent, which indicates that the impurity atoms have relatively little effect on the structural deformation of H_2S from the initial state (IS) to the

Table 5. Dissolution Energy Barrier (E_{dif}) and Reaction Heat (ΔE) of H Diffusion on the Pristine and Those Preadsorbed with Impurity Atom Fe(100) Surfaces

diffusion pathways	exclude ZPE correction		include ZPE correction	
	E_{dif} (eV)	ΔE (eV)	$E_{dif-ZPE}$ (eV)	ΔE_{-ZPE} (eV)
pristine Fe(100) surface				
$Path_1$: H → G_1	0.35	0.34	0.38	0.37
$Path_2$: G_1 → G_2	**0.56**	0.48	**0.56**	0.47
$Path_3$: H → G_2	0.83	0.83	0.86	0.85
Fe(100)−H surface				
$Path_1$: H → G_1	0.29	0.29	0.32	0.33
$Path_2$: G_1 → G_2	**0.56**	0.52	**0.56**	0.50
$Path_3$: H → G_2	0.83	0.81	0.86	0.83
Fe(100)−O surface				
$Path_1$: H → G_1	0.34	0.32	0.37	0.35
$Path_2$: G_1 → G_2	**0.62**	0.61	**0.62**	0.59
$Path_3$: H → G_2	1.03	0.93	1.07	0.95
Fe(100)−S surface				
$Path_1$: H → G_1	0.35	0.34	0.38	0.37
$Path_2$: G_1 → G_2	**0.54**	0.50	**0.54**	0.49
$Path_3$: H → G_2	0.94	0.84	0.98	0.86

https://doi.org/10.1021/acsomega.1c01946
ACS Omega 2021, 6, 14701−14712

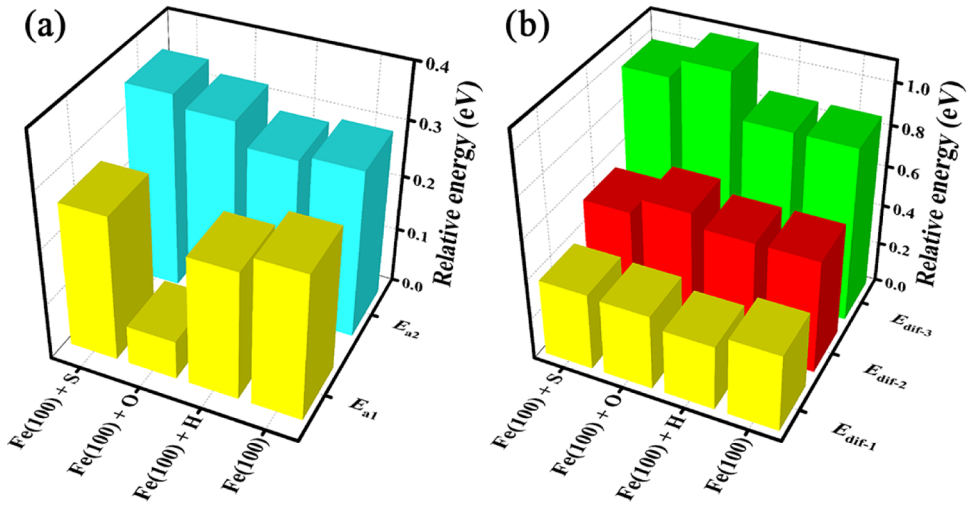

Figure 8. Dissociation barrier (E_a) of H_2S (a) and the diffusion barrier (E_{dif}) of H atoms (b) on the pristine and those preadsorbed with H, O, and S atom Fe(100) surfaces.

Table 6. Energy Value of Each Part after the Maximum Dissociation E_a of H_2S[a]

ΔE_{slab} (eV)	ΔE_{def-H_2S} (eV)	$E_{IS_1}^{H_2S}$ (eV)	$E_{TS_1}^{H}$ (eV)	$E_{TS_1}^{HS}$ (eV)	$E_{int-H\cdots HS}$ (eV)
	pristine Fe(100): (I) $H_2S_{ads} \rightarrow H_{ads} + HS_{ads}$				
0.01	0.09	−0.56	0.38	−2.88	−2.1
	Fe(100)−H: (I) $H_2S_{ads} \rightarrow H_{ads} + HS_{ads}$				
−0.03	0	−0.49	**2.49**	−3.05	**−0.34**
	Fe(100)−O: (I) $H_2S_{ads} \rightarrow H_{ads} + HS_{ads}$				
−0.02	0.06	**−0.35**	0.53	−2.79	−1.94
	Fe(100)−S: (I) $H_2S_{ads} \rightarrow H_{ads} + HS_{ads}$				
0.02	0.03	−0.45	**2.32**	−3.2	**−0.64**

[a]Black bold font indicates the greatest impact on dissociation E_a.

Table 7. Energy Value of Each Part after the Maximum Dissociation E_a of HS[a]

ΔE_{slab} (eV)	ΔE_{def-HS} (eV)	$E_{IS_2(3)}^{HS}$ (eV)	$E_{TS_2(3)}^{H}$ (eV)	$E_{TS_2(3)}^{S}$ (eV)	$E_{int-H\cdots S}$ (eV)
	pristine Fe(100): (II) $HS_{ads} \rightarrow Ha_{ds} + Sa_{ds}$				
0	0.05	−3.86	2.82	−2.89	3.54
	Fe(100)−H: (II) HSads → Hads + Sads				
0.03	0.03	−3.86	**2.57**	**−2.55**	**3.64**
	Fe(100)−O: (II) $HS_{ads} \rightarrow Ha_{ds} + Sa_{ds}$				
0.02	0.04	−3.82	2.78	−2.9	**3.43**
	Fe(100)−S: (II) $HS_{ads} \rightarrow Ha_{ds} + Sa_{ds}$				
0	0.05	−3.86	**2.74**	**−2.8**	3.5

[a]Black bold font indicates the greatest impact on dissociation E_a

TS. Besides, O and S atoms have a more significant influence on the adsorption energy of H_2S. This is caused by the difference between the adsorption site of H_2S on the preadsorbed O/S atoms and the pristine Fe(100) surface.

The reduction in adsorption energy is conducive to reducing the decomposition of H_2S and the contribution of this part to E_a is most evident on the surface adsorbed with the O atom. The adsorption energy of the H atom in TS_1 increases by 2.11 and 1.94 eV on Fe(100)−H and Fe(100)−S surfaces, respectively. This has the greatest contribution to the dissociation barrier compared to the pristine surface. However, the interaction energy between H and HS ($E_{int-H\cdots HS}$) has an immense negative contribution to E_a, which can offset a part of the positive contribution of the adsorption energy of the H atom. As a result, the E_a of H_2S on Fe(100)−H and Fe(100)−S surfaces does not change significantly compared to that on the pristine surface.

The adsorption energy of the S atom decreases obviously, while that of the H atom increases and the interaction energy between S and H atoms also increases on the Fe(100)−H surface. This indicates that the impurity H atom significantly reduces the interaction of the S atom and substrate, but the interaction energy between H and S atoms as well as the increase of adsorption energy of the H atom will cancel out the change of adsorption energy of the S atom, thus making the dissociation barrier E_a change less obvious. The impurity O atom will decrease the energy of interaction between S and H atom in the TS, which is the main reason for the increase of the HS dissociation barrier. The impurity S atom will reduce the adsorption energy of the S atom in the TS. This may be due to the large repulsion between the impurity atom and S atom, which hinders the dissociation process of HS.

It can be seen that the impact of impurity atoms on the dissociation of E_a of H_2S/HS is manifold. On different surfaces of impurity atoms, the contribution of different parts to E_a is very different. Many factors determine the change of E_a and changes in factors do not necessarily cause E_a to increase or decrease.

3. COMPUTATIONAL DETAILS

3.1. Models. The body-centered cubic structure is used for iron lattice modeling. After geometric optimization, the lattice constant is calculated as 2.831 Å for a, b, and c, which is only 1.22% error compared with the experimental results of 2.866 Å.[28] The slab model constructed in this chapter adopts a 3 × 3 supercell structure and sets four atomic layers to adapt to the relaxation inflation of the first surface layer.[29] An additional 15 Å vacuum layer is placed to ensure separation.

For H_2S in the gas phase and bulk Fe calculations, the Monkhorst−Pack algorithm is used with a grid size of 13 × 13 × 13 mesh of *k*-points, while 3 × 3 × 1 is applied for Fe(100) surface calculations.[30] By adding spin polarization parameters,

https://doi.org/10.1021/acsomega.1c01946
ACS Omega 2021, 6, 14701−14712

the magnetic moment of iron calculated in this study is 2.21 μB, which is not only completely in conformity with the previous theoretical calculation value 2.21−2.23 μB[31] but also approximate to the corresponding experimental value (2.22 μB),[32] thus laying the foundation for the study of surface properties. During the calculation, the bottom layer is fixed and the other three layers are relaxed to balance. In this study, the ZPE correction is implemented on the adsorption energy and dissociation barrier, which has a significant impact on gas molecules.[33,34]

3.2. Methods. The structures and total energies are executed using the plane-wave DFT calculations with the Vienna Ab-initio Simulation Package (VASP).[35−38] The electron−ion interactions are described by the projector augmented wave method and the electron−electron exchange−correlation interactions are performed by the generalized gradient approximation using the functional of Perdew−Burke−Ernzerhof.[39−41] Simultaneously, in order to calculate ferromagnetism correctly, spin polarization parameters are added in the calculation process, which is essential to describe the adsorption process accurately.[42,43] A cutoff energy of 400 eV is tested and the cutoff energy is sufficient to converge the total energy of all systems. The convergence standards of energy and force are 10^{-5} eV and 0.05 eV·Å^{-1}, respectively.

CI-NEB[44,45] is used to search the TS of the dissociation process of H_2S and HS accurately, while six intermediate states are inserted between the final state (FS) and IS to ensure that the TS is searched precisely. Then, the frequency of the TS is verified to ensure that there is only one virtual frequency.

The adsorption energy of molecules/atoms on the surface and the energy correction of ZPE are defined by the following formula, respectively[46,47]

$$E_{ads/dis} = E_{X/slab} - E_{slab} - E_X \quad (1)$$

$$E_{ads/dis-ZPE} = (E_{X/slab} + E_{ZPE}) - E_{slab} - (E_X + E_{ZPE}) \quad (2)$$

Here, $E_{X/slab}$, E_{slab}, and E_X denote the total adsorption/dissolution energy of the surface, independent slab model of the surface, and isolated gas-phase molecules/atoms. These three types of energy are obtained through optimization using the same cyclical slab model and parameter settings. Therefore, a positive value of $E_{ads/dis}$ indicates an endothermic reaction, which is not conducive to the adsorption or dissolution process, while a negative value represents an exothermic reaction and is conducive to the occurrence of the adsorption/dissolution process.

The correction of ZPE can be calculated by the vibration frequency[48]

$$E_{ZPE} = \frac{1}{2}\sum_{j=1}^{3n} h\nu_j \quad (3)$$

where ν_j is the real vibration frequency and h stands for the Planck constant. To better understand the interaction between H_2S and the slab model of the Fe(100) surface, PDOS is used to analyze the electronic structure before and after the interaction. It can determine the type of bonding more accurately between H_2S and the iron surface.

The activation energy barrier (ΔE) and the reaction heat (E_a) of the dissociation process of H_2S and HS are defined by the following formulas, respectively[49,50]

$$\Delta E = E_{FS} - E_{IS} \quad (4)$$

$$E_a = E_{TS} - E_{IS} \quad (5)$$

where E_{FS}, E_{IS}, and E_{TS} are the relevant FS, IS, and TS energy during the dissociation process.

The following formulas are used to decompose the calculated energy barriers E_{a1} and E_{a2}[51]

$$E_{a1} = \Delta E_{slab} + \Delta E_{def\text{-}H_2S} - E_{IS_1}^{H_2S} + E_{TS_1}^{H} + E_{TS_1}^{HS} - E_{int\text{-}H\cdots HS} \quad (6)$$

$$E_{a2} = \Delta E_{slab} + \Delta E_{def\text{-}HS} - E_{IS_i}^{HS} + E_{TS_i}^{H} + E_{TS_i}^{S} - E_{int\text{-}H\cdots S} \quad (7)$$

where $\Delta E_{slab} = E_{TS\text{-}slab} - E_{IS\text{-}slab}$ measures the change of slab models from IS to TS. $\Delta E_{def\text{-}H_2S}$ and $\Delta E_{def\text{-}HS}$ are distortion energies, which represent the structural deformation of H_2S and HS in the TS. $E_{IS_1}^{H_2S}$ and $E_{IS_i}^{HS}$ are the adsorption energies of H_2S and HS in the initial configuration. $E_{TS_i}^{H}$ and $E_{TS_i}^{S}$ refer to the adsorption energy of H (no HS) and HS (no H) in the TS, while $E_{TS_i}^{H}$ and $E_{TS_i}^{S}$ refer to the adsorption energy of H (no S) and S (no H) in the TS configuration, respectively. $E_{int\text{-}H\cdots HS}$ and $E_{int\text{-}H\cdots S}$ are the reciprocity energies between H and HS and H and S in the TS configuration.

4. CONCLUSIONS

The ubiquitous substances in the working environment (such as H_2S, H_2O, O_2, and H_2 molecules) may dissociate into H, O, S, and other atoms. After a while, these atoms will be adsorbed and affect the adsorption/dissociation of H_2S on the iron surface. In our calculation, the H atom does not change the adsorption site of H_2S but has a slight inhibition on the dissociation of H_2S; the O atom will not only transfer the adsorption site of H_2S from the bridge to the top but also significantly promote the dissociation of H_2S. Compared with the pristine surface (0.28 eV), the first dissociation barrier of H_2S on the Fe(100)−O surface is only 0.07 eV. The energy barrier resolution calculation shows that the main reason for reducing the dissociation barrier is the reduction of the H_2S adsorption energy; the S atom has a large atomic radius and is far from the iron surface after adsorption. The large repulsion force between the S atom and H_2S makes the adsorption site of H_2S transfer to the bridge site further away from the S atom, and the TS configuration of the first-order dissociation is significantly affected. In addition, both O and S atoms will hinder the dissociation of HS. It is worth mentioning that these three kinds of atoms have little influence on the diffusion process of the H atom to the subsurface. Our research investigated the effect of impurity atoms (H, O, and S) on the adsorption/dissociation of H_2S and H diffusion behavior during the initial stage of H_2S corrosion with steel in the actual environment. The influence mechanism of impurity atoms on the adsorption/dissociation of H_2S and H diffusion from the surface to subsurface on the Fe(100) surface is theoretically explained. In summary, this work could provide some theoretical basis for the corrosion process of steel in a H_2S environment.

https://doi.org/10.1021/acsomega.1c01946
ACS Omega 2021, 6, 14701−14712

■ ASSOCIATED CONTENT

Supporting Information

The Supporting Information is available free of charge at https://pubs.acs.org/doi/10.1021/acsomega.1c01946.

PDOS of the isolated H_2S and free Fe(100) surface slab model; top view of the intermediate state and the TS of the most favorable path for the dissociation of H_2S and HS on the pristine Fe(100) surface, including ZPE correction; and adsorption energy, adsorption sites, and structural parameters of HS, H + HS, and H + S adsorbed on different Fe(100) surfaces (PDF)

■ AUTHOR INFORMATION

Corresponding Author

Shuqi Zheng − *State Key Laboratory of Heavy Oil Processing, Department of Materials Science and Engineering, China University of Petroleum (Beijing), Beijing 102249, PR China;* orcid.org/0000-0003-1549-8000; Phone: +86 010 8973 3200; Email: zhengsq09@163.com; Fax: +86 010 8973 3200

Authors

Jingxuan Liang − *State Key Laboratory of Heavy Oil Processing, Department of Materials Science and Engineering, China University of Petroleum (Beijing), Beijing 102249, PR China*

Xiangli Wen − *State Key Laboratory of Heavy Oil Processing, Department of Materials Science and Engineering, China University of Petroleum (Beijing), Beijing 102249, PR China; State Key Laboratory of Tribology, Department of Mechanical Engineering, Tsinghua University, Beijing 100084, PR China*

Shikai Wei − *State Key Laboratory of Heavy Oil Processing, Department of Materials Science and Engineering, China University of Petroleum (Beijing), Beijing 102249, PR China*

Complete contact information is available at: https://pubs.acs.org/10.1021/acsomega.1c01946

Notes

The authors declare no competing financial interest.

■ ACKNOWLEDGMENTS

This work was financially supported by the National Natural Science Foundation of China (no. 51671215). The calculations were carried out at the National Supercomputing Center in Shenzhen (Shenzhen Cloud Computing Center).

■ REFERENCES

(1) Lauretta, D. S.; Lodders, K.; Fegley, B. Experimental simulations of sulfide formation in the solar nebula. *Science* **1997**, *277*, 358−360.

(2) Bai, P.; Zheng, S.; Zhao, H.; Ding, Y.; Wu, J.; Chen, C. Investigations of the diverse corrosion products on steel in a hydrogen sulfide environment. *Corros. Sci.* **2014**, *87*, 397−406.

(3) Bai, P.; Zhao, H.; Zheng, S.; Chen, C. Initiation and developmental stages of steel corrosion in wet H_2S environments. *Corros. Sci.* **2015**, *93*, 109−119.

(4) Zhou, E.; Wang, J.; Moradi, M.; Li, H.; Xu, D.; Lou, Y.; Luo, J.; Li, L.; Wang, Y.; Yang, Z.; Wang, F.; Smith, J. A. Methanogenic archaea and sulfate reducing bacteria induce severe corrosion of steel pipelines after hydrostatic testing. *J. Mater. Sci. Technol.* **2020**, *48*, 72−83.

(5) Brunner, E.; Woll, W. Solubility of sulfur in hydrogen sulfide and sour gases. *Soc. Pet. Eng. J.* **1980**, *20*, 377−384.

(6) Wen, X.; Bai, P.; Luo, B.; Zheng, S.; Chen, C. Review of recent progress in the study of corrosion products of steels in a hydrogen sulphide environment. *Corros. Sci.* **2018**, *139*, 124−140.

(7) Li, Y.; Huang, P.; Tao, D.; Wu, J.; Qiu, M.; Huang, X.; Ding, K.; Chen, W.; Su, W.; Zhang, Y. Adsorption and dissociation of H_2S on monometallic and monolayer bimetallic Ni/Pd(111) surfaces: A first-principles study. *Appl. Surf. Sci.* **2016**, *387*, 301−307.

(8) Wen, X.; Liang, Y.; Bai, P.; Luo, B.; Fang, T.; Yue, L.; An, T.; Song, W.; Zheng, S. First-principles calculations of the structural, elastic and thermodynamic properties of mackinawite (FeS) and pyrite (FeS_2). *Phys. B* **2017**, *525*, 119−126.

(9) Bai, P.; Liang, Y.; Zheng, S.; Chen, C. Effect of Amorphous FeS Semiconductor on the Corrosion Behavior of Pipe Steel in H_2S-Containing Environments. *Ind. Eng. Chem. Res.* **2016**, *55*, 10932−10940.

(10) Mohtadi-Bonab, M. A.; Szpunar, J. A.; Basu, R.; Eskandari, M. The mechanism of failure by hydrogen induced cracking in an acidic environment for API 5L X70 pipeline steel. *Int. J. Hydrogen Energy* **2015**, *40*, 1096−1107.

(11) Krishnamoorthy, A.; Dinh, M. A.; Yildiz, B. Hydrogen weakens interlayer bonding in layered transition metal sulfide $Fe_{1+x}S$. *J. Mater. Chem. A* **2017**, *5*, 5030−5035.

(12) Jiang, D. E.; Carter, E. A. Adsorption, diffusion, and dissociation of H_2S on Fe(100) from first principles. *J. Phys. Chem. B* **2004**, *108*, 19140−19145.

(13) Jiang, D. E.; Carter, E. A. First principles study of H_2S adsorption and dissociation on Fe(110). *Surf. Sci.* **2005**, *583*, 60−68.

(14) Luo, Q.; Tang, B.; Zhang, Z.; Ran, Z-L. First principles calculation of adsorption for H_2S on Fe(100) surface. *Acta Phys. Sin.* **2013**, *62*, 077101.

(15) Feng-Chun, Z.; Chun-Fu, L.; Cong-Lei, Z.; Zeng-Ling, R. Surface absorptions of H_2S, HS and S on Fe(111) investigated by density functional theory. *Acta Phys. Sin.* **2014**, *63*, 127101−127130.

(16) Wen, X.; Bai, P.; Han, Z.; Zheng, S.; Luo, B.; Fang, T.; Song, W. Effect of vacancy on adsorption/dissociation and diffusion of H_2S on Fe(100) surfaces: A density functional theory study. *Appl. Surf. Sci.* **2019**, *465*, 833−845.

(17) Wang, T.; Tian, X.; Li, Y.-W.; Wang, J.; Beller, M.; Jiao, H. High Coverage CO Activation Mechanisms on Fe(100) from Computations. *J. Phys. Chem. C* **2014**, *118*, 1095−1101.

(18) Liu, S.; Tian, X.; Wang, T.; Wen, X.; Li, Y.-W.; Wang, J.; Jiao, H. High Coverage Water Aggregation and Dissociation on Fe(100): A Computational Analysis. *J. Phys. Chem. C* **2014**, *118*, 26139−26154.

(19) Liu, S.; Tian, X.; Wang, T.; Wen, X.; Li, Y.-W.; Wang, J.; Jiao, H. Coverage dependent water dissociative adsorption on Fe(110) from DFT computation. *Phys. Chem. Chem. Phys.* **2015**, *17*, 8811−8821.

(20) Liu, S.; Li, Y.-W.; Wang, J.; Jiao, H. Reactions of CO, H_2O, CO_2, and H_2 on the Clean and Precovered Fe(110) Surfaces − A DFT Investigation. *J. Phys. Chem. C* **2015**, *119*, 28377−28388.

(21) Liu, S.; Li, Y.-W.; Wang, J.; Jiao, H. Reaction of CO, H_2O, H_2 and CO_2 on the clean as well as O, OH and H precovered Fe(100) and Fe(111) surfaces. *Catal. Sci. Technol.* **2017**, *7*, 427−440.

(22) Tao, S.-X.; Wang, G.-C.; Bu, X.-H. Effect of pre-covered oxygen on the dehydrogenation reactions over copper surface: A density functional theory study. *J. Phys. Chem. B* **2006**, *110*, 26045−26054.

(23) Hao, G.; Zhang, R.; Li, J.; Wang, B.; Zhao, Q. Insight into the effect of surface structure on H_2 adsorption and activation over different CuO(111) surfaces: A first-principle study. *Comput. Mater. Sci.* **2016**, *122*, 191−200.

(24) Abbasi, A.; Sardroodi, J. J. Adsorption and dissociation of H_2S on nitrogen-doped TiO_2 anatase nanoparticles: Insights from DFT computations. *Surf. Interfaces* **2017**, *8*, 15−27.

(25) Thiel, P. A.; Madey, T. E. The interaction of water with solid surfaces: fundamental aspects. *Surf. Sci. Rep.* **1987**, *7*, 211−385.

(26) Han, Z.; Yu, H.; Li, C.; Zhou, S. Mulch-assisted ambient-air synthesis of oxygen-rich activated carbon for hydrogen storage: A combined experimental and theoretical case study. *Appl. Surf. Sci.* **2021**, *544*, 148963.

(27) Han, Z.; Wu, Y.; Yu, H.; Zhou, S. Location-dependent effect of nickel on hydrogen dissociation and diffusion on Mg (0001) surface: Insights into hydrogen storage material design. *J. Magnesium Alloys* **2021**, DOI: 10.1016/j.jma.2021.03.002.
(28) Kittel, C. *Introduction to solid state physics*; Wiley, 1976.
(29) Liang, T.; Kang, H.; Zhong, W.; Bian, H.; Zhao, J. Impact of surface adsorbed gases on hydrogen diffusion into Pd(100) subsurface from first principles. *Appl. Surf. Sci.* **2019**, *473*, 476−485.
(30) Chadi, D. J. Special points for Brillouin-zone integrations. *Phys. Rev. B: Solid State* **1977**, *16*, 1746−1747.
(31) Jung, S. C.; Kang, M. H. Adsorption of a water molecule on Fe(100): Density-functional calculations. *Phys. Rev. B: Condens. Matter Mater. Phys.* **2010**, *81*, 115460.
(32) Herper, H. C.; Hoffmann, E.; Entel, P. Ab initio full-potential study of the structural and magnetic phase stability of iron. *Phys. Rev. B: Condens. Matter Mater. Phys.* **1999**, *60*, 3839−3848.
(33) Liu, A.; Long, J.; Yuan, S.; Cen, W.; Li, J. Synergetic promotion by oxygen doping and Ca decoration on graphene for CO_2 selective adsorption. *Phys. Chem. Chem. Phys.* **2019**, *21*, 5133−5141.
(34) Vakili, M.; Gholizadeh, R.; Ghadi, A.; Salmasi, E.; Sinnokrot, M. Computational investigation of N_2O adsorption and dissociation on the silicon-embedded graphene catalyst: A density functional theory perspective. *J. Mol. Graphics Modell.* **2020**, *101*, 107752.
(35) Kresse, G.; Furthmüller, J. Efficiency of ab-initio total energy calculations for metals and semiconductors using a plane-wave basis set. *Comput. Mater. Sci.* **1996**, *6*, 15−50.
(36) Kresse, G.; Furthmüller, J. Efficient iterative schemes for ab initio total-energy calculations using a plane-wave basis set. *Phys. Rev. B: Condens. Matter Mater. Phys.* **1996**, *54*, 11169−11186.
(37) Kresse, G.; Hafner, J. Ab initio molecular dynamics for open-shell transition metals. *Phys. Rev. B: Condens. Matter Mater. Phys.* **1993**, *48*, 13115−13118.
(38) Kresse, G.; Hafner, J. Norm-conserving and ultrasoft pseudopotentials for first-row and transition elements. *J. Phys.: Condens. Matter* **1994**, *6*, 8245−8257.
(39) Blöchl, P. E. Projector augmented-wave method. *Phys. Rev. B: Condens. Matter Mater. Phys.* **1994**, *50*, 17953−17979.
(40) Kresse, G.; Joubert, D. From ultrasoft pseudopotentials to the projector augmented-wave method. *Phys. Rev. B: Condens. Matter Mater. Phys.* **1999**, *59*, 1758−1775.
(41) Wei, S.; Zheng, S.; Xie, C.; Liang, J. Ab initio molecular dynamics study of wet H_2S adsorption and dissociation on Fe(100) surface. *J. Mol. Liq.* **2020**, *319*, 114135.
(42) Wei, S.; Zheng, S.; Wen, X.; Xie, C.; Liang, J. A novel antiferromagnetic semiconductor hidden in pyrite. *Comput. Mater. Sci.* **2020**, *183*, 109852.
(43) Koo, H.-J.; Whangbo, M.-H. Effect of Nonmagnetic Ion Deficiency on Magnetic Structure: Density Functional Study of $Sr_2MnO_2Cu_{2-x}Te_2$, $Sr_2MO_2Cu_2Te_2$ (M = Co, Mn), and the Oxide-Hydrides Sr_2VO_3H, $Sr_3V_2O_5H_2$, and $SrVO_2H$. *Inorg. Chem.* **2019**, *58*, 14769−14776.
(44) Xing, H.; Hu, P.; Li, S.; Zuo, Y.; Han, J.; Hua, X.; Wang, K.; Yang, F.; Feng, P.; Chang, T. Adsorption and diffusion of oxygen on metal surfaces studied by first-principle study: A review. *J. Mater. Sci. Technol.* **2021**, *62*, 180−194.
(45) Wen, X.; Bai, P.; Zheng, S.; Tian, Y. Adsorption and dissociation mechanism of hydrogen sulfide on layered FeS surfaces: A dispersion-corrected DFT study. *Appl. Surf. Sci.* **2021**, *537*, 147905.
(46) Belghiti, M. E.; Mihit, M.; Mahsoune, A.; Elmelouky, A.; Mghaiouini, R.; Barhoumi, A.; Dafali, A.; Bakasse, M.; El Mhammedi, M. A.; Abdennouri, M. Studies of Inhibition effect "E & Z" Configurations of hydrazine Derivatives on Mild Steel Surface in phosphoiric acid. *J. Mater. Res. Technol.* **2019**, *8*, 6336−6353.
(47) Pham, N. N. T.; Kang, S. G.; Kim, H.-J.; Pak, C.; Han, B.; Lee, S. G. Catalytic activity of Ni_3Mo surfaces for hydrogen evolution reaction: A density functional theory approach. *Appl. Surf. Sci.* **2021**, *537*, 147894.
(48) Boda, A.; Ali, S. M.; Shenoy, K. T.; Mohan, S. Adsorption, Absorption, Diffusion, and Permeation of Hydrogen and Its Isotopes in bcc Bulk Fe and Fe(100) Surface: Plane Wave-Based Density Functional Theoretical Investigations. *J. Phys. Chem. C* **2019**, *123*, 23951−23966.
(49) Lei, S.; Guo, S.; Sun, X.; Yu, H.; Xu, F.; Wan, N.; Wang, Z. Capture and dissociation of dichloromethane on Fe, Ni, Pd and Pt decorated phosphorene. *Appl. Surf. Sci.* **2019**, *495*, 143533.
(50) Liu, J.; Yang, T.; Peng, Q.; Yang, Y.; Li, Y.-W.; Wen, X.-D. Theoretical exploration of the interaction between hydrogen and pyrite-type FeS_2 surfaces. *Appl. Surf. Sci.* **2021**, *537*, 147900.
(51) Cao, Y.; Chen, Z.-X. Slab model studies of water adsorption and decomposition on clean and X- (X = C, N and O) contaminated Pd(111) surfaces. *Phys. Chem. Chem. Phys.* **2007**, *9*, 739−746.